Int. J. Radiation Oncology Biol. Phys., Vol. 58, No. 5, pp. 1584–1595, 2004

0360-3016/04/$–see front matter

ELSEVIER

doi:10.1016/j.ijrobp.2003.09.077

PHYSICS CONTRIBUTION

QUANTIFICATION OF RESPIRATION-INDUCED ABDOMINAL TUMOR MOTION AND ITS IMPACT ON IMRT DOSE DISTRIBUTIONS

DAVID P. GIERGA, PH.D.,* GEORGE T. Y. CHEN, PH.D.,* JONG H. KUNG, PH.D.,* MARGRIT BETKE, PH.D.,† JONATHAN LOMBARDI, M.S.,† AND CHRISTOPHER G. WILLETT, M.D.*

*Department of Radiation Oncology, Massachusetts General Hospital, Boston, MA; †Department of Computer Science, Boston University, Boston, MA

Purpose: The treatment of moving targets with intensity-modulated radiotherapy may introduce errors in dose delivery. The motion of tumors in the abdomen was studied using quantitative fluoroscopic analysis, and the effect on dose delivery to the target was studied.

Methods and Materials: Fluoroscopy sessions for 7 patients with pancreas or liver tumors and fiducial clips were recorded, converted to digital format, and analyzed to quantify the characteristics of tumor motion. Intensity-modulated radiotherapy plans were generated for 3 patients (a total of five plans), and the dose–volume histograms for the target volume were compared between plans with and without tumor motion.

Results: The average magnitude of the peak-to-peak motion for the 7 patients in the craniocaudal and AP directions was 7.4 mm and 3.8 mm, respectively. The clip motion varied widely, because the maximal clip excursions were about 47% greater than the average clip excursions for each patient. The inclusion of tumor motion did not lead to a significant degradation in the target dose–volume histogram for four of five treatment plans studied.

Conclusion: The amount of tumor motion for most patients in this study was not large but could, in some instances, significantly degrade the planned target dose–volume histogram. For some patients, therefore, motion mitigation or intervention during treatment may be necessary. © **2004 Elsevier Inc.**

IMRT, Fluoroscope, Abdomen, Motion, Tracking.

INTRODUCTION

Intensity-modulated radiotherapy (IMRT) is a technique used to deliver radiation conformally to tumor volumes while simultaneously sparing organs at risk. IMRT has been used to treat many sites, including the head and neck, prostate, lung, and juxtaspinal sarcomas. The understanding and potential mitigation of target motion during IMRT delivery is crucial to ensuring accurate delivery. Target motion during the delivery of IMRT may lead to a degradation of the planned dose distribution in two ways. The first source of error is simply from inadequate margins (i.e., planning target volume [PTV] not large enough to encompass target excursions). The delineation of the PTV margins is a balance between adequate target coverage and critical structure sparing, particularly when IMRT is used to spare critical structures adjacent to the target. The second, and subtler, effect of target motion during IMRT delivery is in the interplay between dynamic multileaf collimator motion and intrafractional tumor motion. This effect may lead to significant differences between planned and delivered dose distributions.

Intrafractional target motion caused by respiration is a particular concern for lung and abdominal tumors. The magnitude of respiration-induced target motion can be as large as 2–3 cm, peak-to-peak. Various methods have been proposed to control or mitigate target motion in the lung. These include active or passive breath-hold techniques (1–4), respiratory gating (5–8), and tumor tracking (9–11). The extent of target motion for abdominal tumors and the impact of target motion on IMRT dose delivery, however, have not been as extensively studied. The purpose of this study was to quantify the respiratory motion for abdominal tumors and to estimate the corresponding effect on the dose–volume histograms (DVHs) of IMRT plans. An improved understanding of the effects of organ motion during respiration may lead to selecting the appropriate strategy, if any, for mitigation of these effects.

The abdominal tumors of interest for this analysis were the pancreas and liver. Applying IMRT to pancreatic or

Reprint requests to: David P. Gierga, Ph.D., Department of Radiation Oncology, Massachusetts General Hospital, Fruit St., Cox 8, Boston, MA 02114. Tel: (617) 724-2274; Fax: (617) 726-3603; E-mail: dgierga@partners.org

Acknowledgments—The authors thank Khaled Aljarrah, Winnifred Wong, and George Masganas for their assistance in the early analysis of the fluoroscopic clip data for several patients.

Received Feb 7, 2003, and in revised form Jul 18, 2003. Accepted for publication Sep 22, 2003.

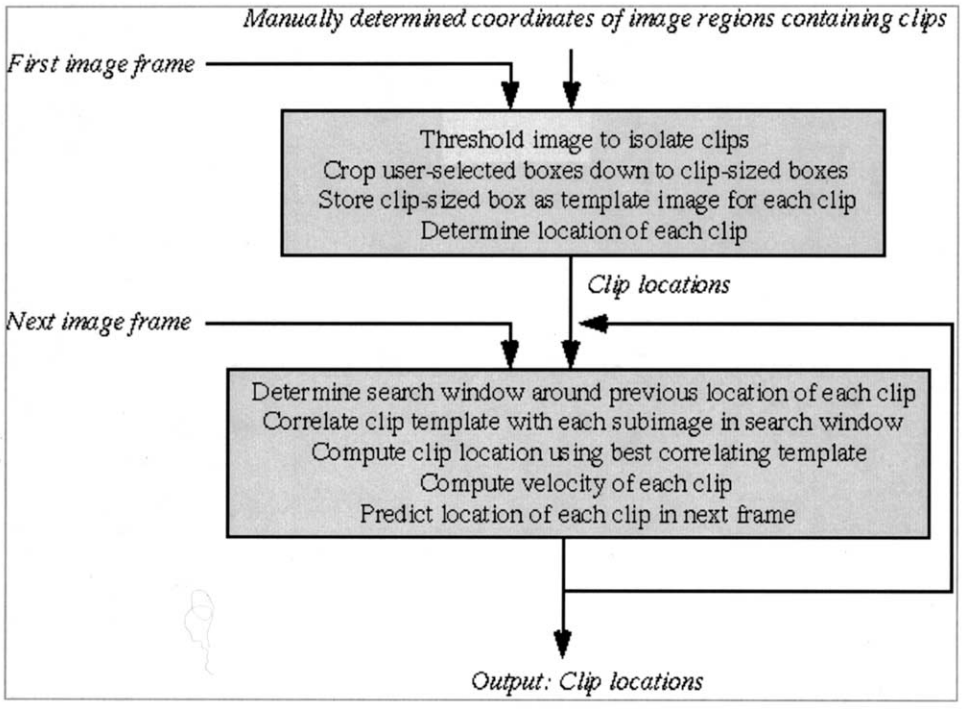

Fig. 1. Flowchart of fluoroscopic video analysis illustrating image processing and recursive filtering techniques.

liver cancer may lead to increased sparing of organs at risk in the abdomen, particularly the kidneys and normal liver (12, 13). In this study, abdominal tumor motion was characterized, and the effect of tumor motion on the IMRT plans was quantified. It should be noted that the motion of interest in this study was intrafraction motion (i.e., the motion of the target during a single fraction while the beam was on). This work did not address interfraction motion (i.e., the day-to-day variation in patient setup and tumor position). The characteristics of tumor motion were studied using fluoroscopy for several patients, with radiopaque clips placed around the tumor site. For pancreatic cancer patients who undergo surgical resection, the surgeon often places clips around the tumor site to denote the area at risk. These clips serve as an aid for the radiation oncologist in designating the clinical target volume (CTV) during patient simulation and treatment planning. In other cases in which tumor motion was a potential concern, clips were placed around the tumor under CT guidance to improve tumor localization. The number of implanted clips can range from about 3 to 10 clips. This paper presents the target motion data for several patients with abdominal tumors. Clip motion was quantified by analyzing each patient's fluoroscopy session, using image processing (14) and recursive filtering (15) techniques to track the motion of the tumor clips. In addition, the effect of tumor motion on the IMRT dose distributions was studied using an effective fluence algorithm developed by Kung *et al.* (16) and Zygmanski *et al.* (17). This algorithm couples the IMRT leaf sequence files generated by the treatment planning system with the patient-specific target motion data to generate an effective fluence, including the effects of target motion. The dosimetric effect of motion was then quantified by DVH comparison for several test cases.

METHODS AND MATERIALS

Patient data

Patients with abdominal tumors and surgically implanted clips were selected for this study. Six patients had pancreatic cancer, and one had cholangiocarcinoma, a tumor located within the liver. All motion analysis and treatment planning comparisons were performed retrospectively. The pancreas cancer patients were all treated with three-dimensional conformal RT, and the patient with liver cancer was treated using IMRT and image guidance with daily diagnostic energy X-ray imaging of the clip positions.

Motion analysis

Patients underwent fluoroscopic simulation to verify the location of the treatment isocenter before beginning RT. Clip motion data were gathered during these sessions by recording the fluoroscopic video signal for about 30 s each for both anterior-posterior (AP) and lateral views. The fluoroscopic images were recorded at a frame rate of 30 frames/s. The AP and lateral views were acquired sequentially, not simultaneously. Data were gathered under normal, free-breathing conditions without any breath control, coaching, or patient instruction. The fluoroscopic session was recorded using a standard video recorder interfaced with the fluoroscopic monitor. These analog videotapes were converted to a digital video format and then analyzed frame by frame as summarized by the algorithm flowchart

in Fig. 1. Software with a graphic user interface was developed at Boston University to view the video and perform the analysis of the fluoroscopy sessions on a desktop computer. The clip tracking software was developed in Visual C++ for the Windows platform. A graphic human–computer interface was implemented. The human operator can view the initial fluoroscopy video frame on the computer screen and use a single mouse click to select the image region that contains the clip. Analysis of subsequent frames was performed automatically. Each user-selected region in the first image frame was processed further to isolate the clip from nearby clips potentially included in the region. A template image of each isolated clip was created and stored for comparison with subimages of the subsequent frames. The location of the isolated clip and the clip template were used to find the location of the clip in the second frame. Because the clip may have moved by a few pixels, the clip was searched for in a window around its previous location. At each position in the search window, the template image was overlaid with the second frame and the normalized correlation coefficient was computed (18). The position of the best correlating template was then used as the estimate for the current clip position and recorded. Given the clip position in the first and second image frame, the clip's velocity was computed and used to predict the location of the clip in the third frame. This process was repeated for the entire fluoroscopy session.

IMRT planning

Iintensity modulated radiation therapy plans were generated using helical CT scans (Lightspeed CT scanner, GE Medical Systems, Waukesha, WI) during normal respiration. An inverse planning system (Helios, version 6.2.7, Varian Medical Systems, Palo Alto, CA) was used to generate optimized treatment plans, ignoring organ motion. The prescription dose for these test cases was either 45 or 50.4 Gy. The CTV was outlined by the radiation oncologist and expanded by 8 mm to the PTV. This expansion should be sufficient for average peak-to-peak target motion of 16 mm (i.e., the amplitude of motion was ± 8 mm from the initial target position). Interfractional setup and the potential dosimetric effects associated with setup uncertainties were not the focus of this study and were not included in the determination of the treatment margins or plan analysis. During inverse planning, the spinal cord dose was limited to 43 Gy, and the volume of the liver and kidney receiving 30 Gy or 20 Gy (or greater), respectively, was minimized using dose–volume constraints. The ranking of the plan objectives was organized as follows: spinal cord tolerance was the highest priority, liver/kidney tolerance was second in priority, and adequate coverage of the tumor was third. Step-and-shoot IMRT plans were generated for a 52-leaf Varian multileaf collimator with 1-cm leaf width at the isocenter. A dose rate of 400 MU/min was used to convert the dynamic leaf motion as a function of cumulative monitor units to leaf motion as a function of cumulative beam on time for each treatment field. An algorithm developed by Kung *et al.* (16) and Zygmanski *et al.* (17) was then used to estimate the effect of organ motion on the original IMRT plan. This algorithm couples the leaf-sequence files generated by the treatment planning system with the patient-specific target motion data, in this case obtained from the fluoroscopic clip analysis. The calculation uses a coordinate transformation into the coordinate system of the moving tumor. In this coordinate, the tumor itself appears stationary, but tumor motion is superimposed on top of the dynamic leaf motion. Patient-specific tumor motion can be modeled (i.e., the motion need not be modeled as simple sinusoidal motion). Tumor motion is approximated as rigid body motion, without deformation. An "effective fluence" is generated for each treatment field and imported into the treatment planning system for use in the three-dimensional dose calculation. The modified IMRT plans, which included the effect of target motion, were then compared with the original plans, which neglected target motion, by comparing the DVHs of the CTV for each plan. DVHs for the PTV were not compared, because the PTV is created to ensure that the CTV receives an adequate dose. Potential changes in the CTV dose, therefore, are the quantity of interest for comparing plans with and without motion.

RESULTS

Fluoroscopy analysis

Fluoroscopic images of pancreatic clip motion as a function of time were obtained for 7 patients. Table 1 summarizes the results of the clip tracking analysis for each patient. The average and maximal peak-to-peak motion in both the craniocaudal (CC) and AP directions are given. The motion in the left–right direction was not analyzed in detail, because the extent of the motion in this direction was <2 mm. The average peak-to-peak motion for either the CC or AP direction was defined as the magnitude of the peak-to-peak motion averaged over all time and all clips for a particular patient. The maximal motion was defined simply as the maximal peak-to-peak motion for any clip recorded for any single breath cycle. For 3 patients, AP motion data were only available for a single clip for a short period, so only the average clip motions are listed in Table 1. The estimated error of the clip tracking algorithm was at most 0.5 mm. This value was derived from the deviations seen in the tracked clip position when the clip was known to be stationary (i.e., at exhale). The average peak-to-peak clip motion, averaged over all clips and all patients, was 7.4 mm in the CC direction and 3.8 mm in the AP direction. The clip motion varied widely over many breath cycles for each patient, and the maximal clip excursions were about 47% greater than the average excursions. The last column in Table 1 lists the standard deviations of the peak-to-peak motion in the CC direction for each patient (calculated from the peak-to-peak motion of each breath cycle observed in the recording interval). For most patients, the standard deviation of clip motion was $<15\%$, ranging from 0.8 to 1.8 mm in absolute terms. For Patient 1, however, the standard

Table 1. Summary of fluoroscopic clip data analysis for 7 patients

Pt. No.	Clip displacement (mm)				Standard deviation of CC peak-to-peak motion (%)
	CC average	CC max	AP average	AP max	
1	9.6	18	6.9	8.7	35–45
2	8.1	9.8	3.9	4.1	5–15
3	12	17	3.0	—	14
4	4.4	6.5	3.6	6.0	9–13
5	4.7	8.0	2.5	6.0	9–15
6	7.3	9.5	4.0	—	21
7	5.6	7.2	3.0	—	11–15

Values listed for average and maximal peak-to-peak motion in craniocaudal (CC) and anterior-posterior (AP) directions; average peak-to-peak motion in left–right direction was <2 mm.

deviation was as much as 45%, corresponding to an uncertainty of >4 mm in the average peak-to-peak motion of 9.6 mm. The average period of motion (not listed in Table 1) was determined to be 3.4 s, with a standard deviation of $\pm 5\%$. The periodicity of motion for all patients was more uniform compared with the amplitude of motion.

Detailed motion data are presented for Patients 1, 2, and 5. These patients were chosen to display a large amount of motion (Patient 1), an average amount of motion (Patient 2), and a small amount of motion (Patient 5). Figure 2 shows the CC motion of four clips for Patient 1. For Fig. 2, the absolute clip positions were offset for display purposes. The maximal peak-to-peak motion for a clip was 1.8 cm; most other clips moved in a range of about 10 mm. Although each clip moved a different amount, all the clips had roughly the same period and followed the same general pattern of motion. Figure 3 shows the corresponding data for the AP direction. The magnitude of motion in this direction was less; the average peak-to-peak motion was about 7 mm. Figures 2 and 3 both show that the breathing pattern was not always stable and reproducible and often included significant deviations from the expected pattern. For clips observed from the AP direction, the peaks observed in the CC direction corresponded to the expiration phase, and the troughs corresponded to inspiration. For clips observed from the lateral view, the peaks corresponded to inspiration, and the troughs corresponded to expiration. From Fig. 2, it is evident that although the amplitude of clip motion varied significantly over many breathing cycles, the expiration position of the clips was nearly constant (± 1 mm). This trend was also evident in Fig. 4, which shows a scatter plot of the exhale (peak) and inhale (trough) data points from Fig. 2.

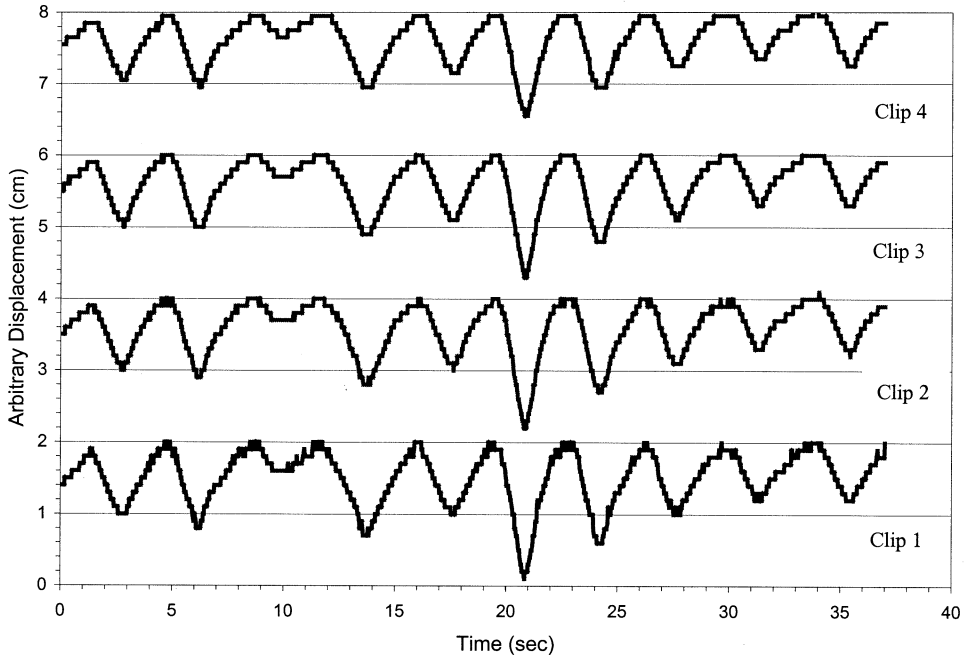

Fig. 2. Cranio-caudal clip motion as a function of time for Patient 1. Absolute values of clip displacements modified for display purposes.

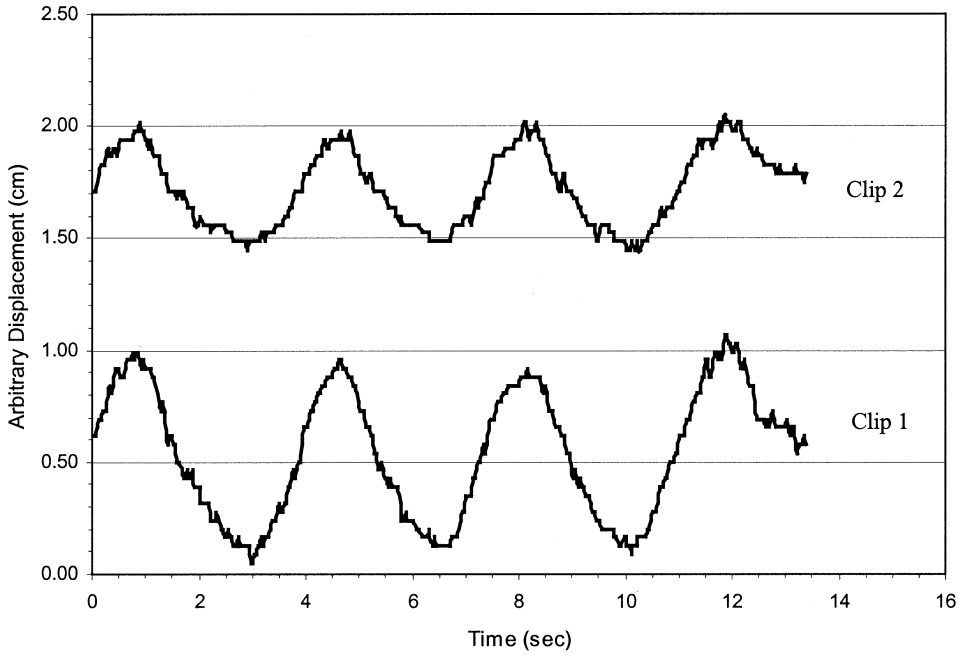

Fig. 3. Anterior-posterio clip motion as a function of time for Patient 1. Absolute values of clip displacements modified for display purposes.

Figure 5 shows the correlation between the CC and AP clip motion for Patient 1, generated from the lateral fluoroscopic movie. The data were plotted over the full range of available breath cycles. These data show a roughly linear correlation between the two directions of motion and illustrate that this correlation is fairly constant with time for this particular patient.

The CC and AP clip motion data for Patient 2 are shown

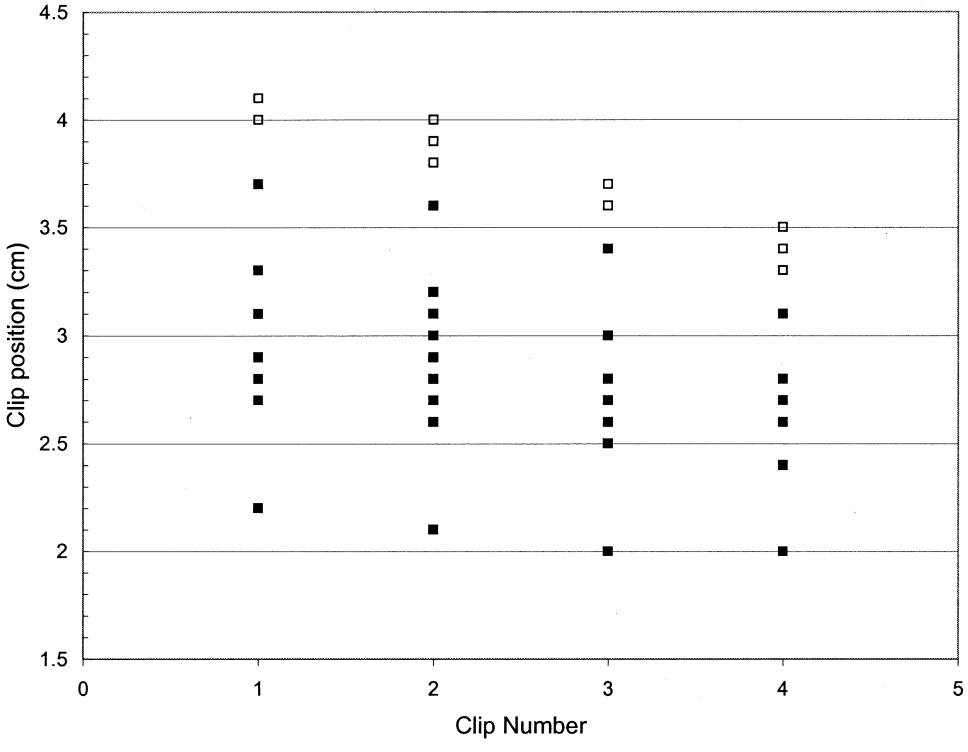

Fig. 4. Scatter plot of exhale (open squares) and inhale (closed squares) for four clips from Patient 1. Data taken from cranio-caudal clip tracking data (anterior-posterior view of patient).

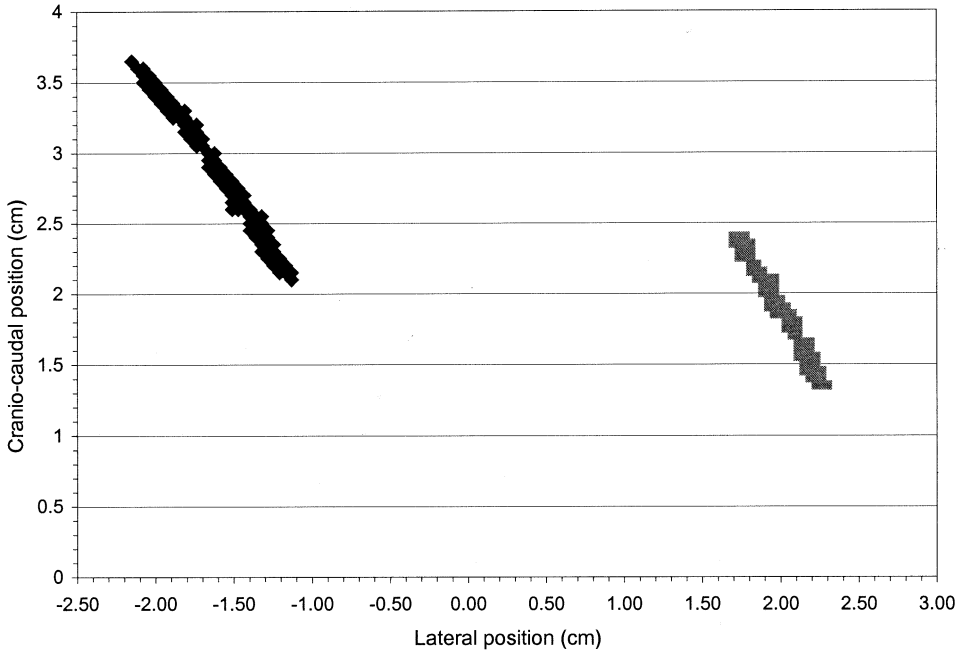

Fig. 5. Cranio-caudal and anterior-posterior motion over several breath cycles for two clips from Patient 1. Data taken from lateral view.

in Figs. 6 and 7, respectively. The average magnitude of clip motion in the CC and AP directions for this case was 8.1 mm and 3.9 mm, respectively. Figure 6 shows that the CC clip motion varied slightly among the clips, with a range of amplitudes of 6–9 mm. The expiration phase of the clip motion was reproducible within 1 mm for all clips. The AP motion for Patient 2 is shown in Fig. 7; both clips behaved similarly, with little variation in amplitude or phase.

Figures 8 and 9 show the clip motion data for Patient 5. The CC motion data showed a statistically significant difference in the magnitude of motion for the three clips. Two of the clips had peak-to-peak amplitudes of about 3.5 mm, and the third had an average amplitude of nearly 7 mm. Similar differences were seen in the AP motion (Fig. 9). The magnitude of clip motion in this direction ranged from 1 to 4.5 mm.

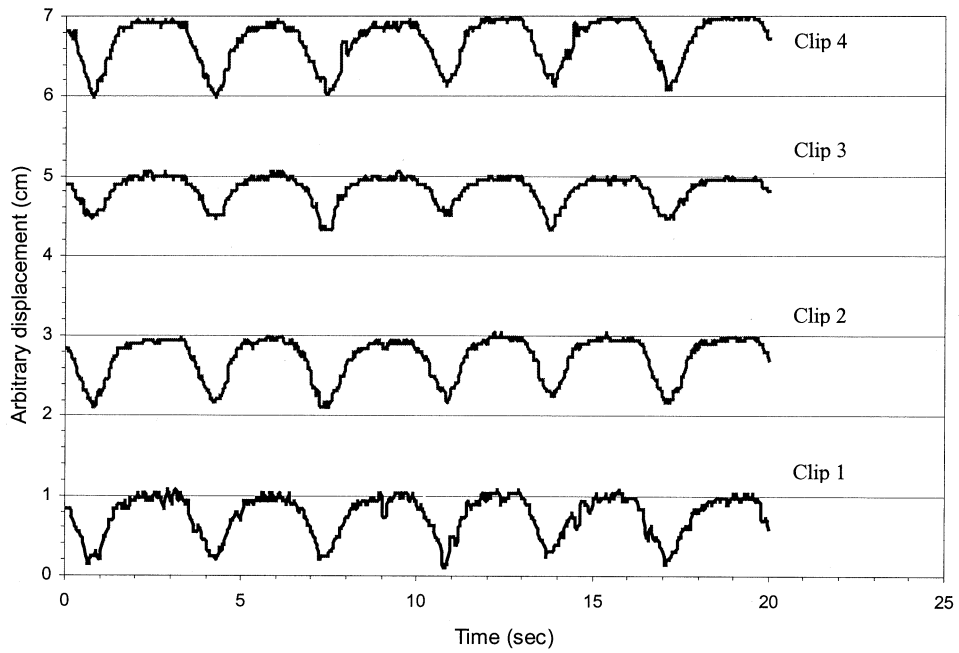

Fig. 6. Cranio-caudal clip motion as a function of time for Patient 2. Absolute values of clip displacements modified for display purposes.

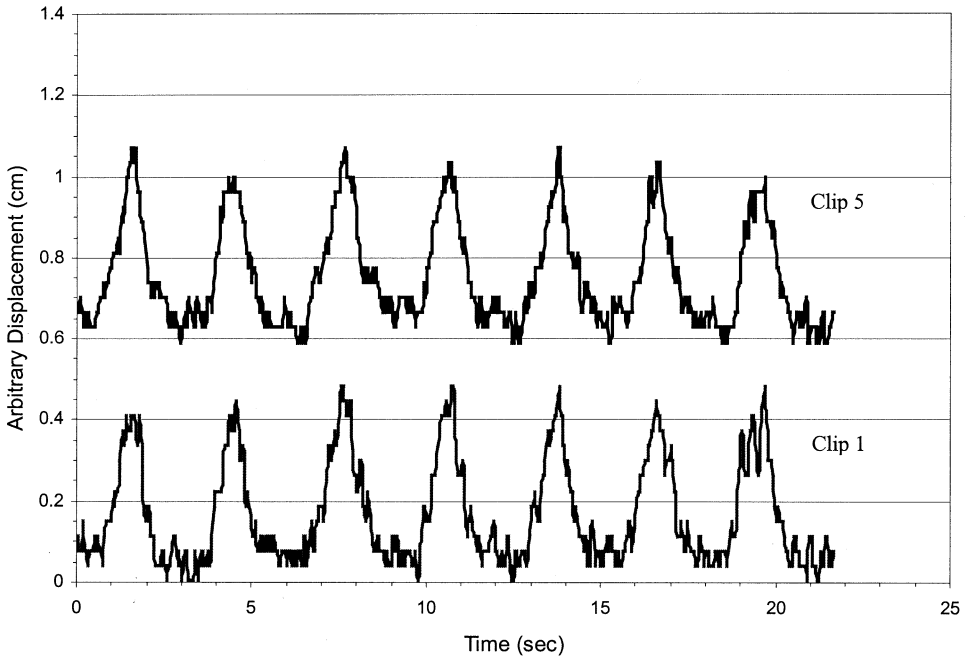

Fig. 7. Anterior-posterior clip motion as a function of time for Patient 2. Absolute values of clip displacements modified for display purposes.

IMRT planning

A comparison of several IMRT plans with and without tumor motion was performed using the algorithm developed by Kung *et al.* (16) and Zygmanski *et al.* (17) and the patient-specific clip motion presented in the previous section. Clip motion data were presented for Patients 1, 2, and 5. These patients were selected because they exhibited large motion (Patient 1), average motion (Patient 2), and small motion (Patient 5). Several treatment planning comparisons were done for Patient 1, who had the largest amount of clip motion. The first two comparisons assumed an artificial target of the body of the pancreas only, and the third comparison used the actual tumor volume at the head of the pancreas, as outlined by the radiation oncologist. Patient 1

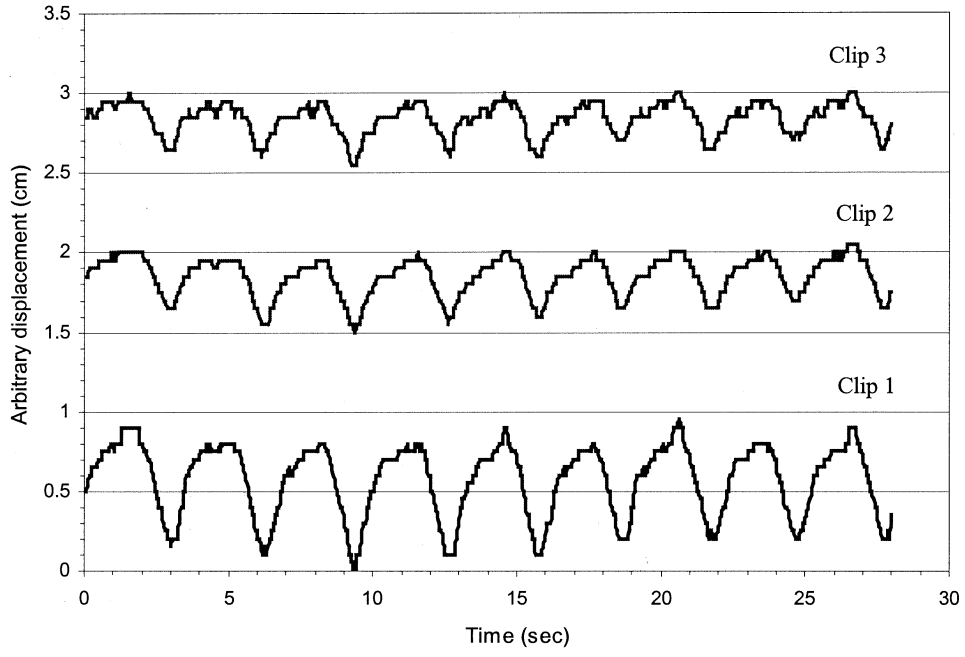

Fig. 8. Cranio-caudal clip motion as a function of time for Patient 5. Absolute values of clip displacements modified for display purposes.

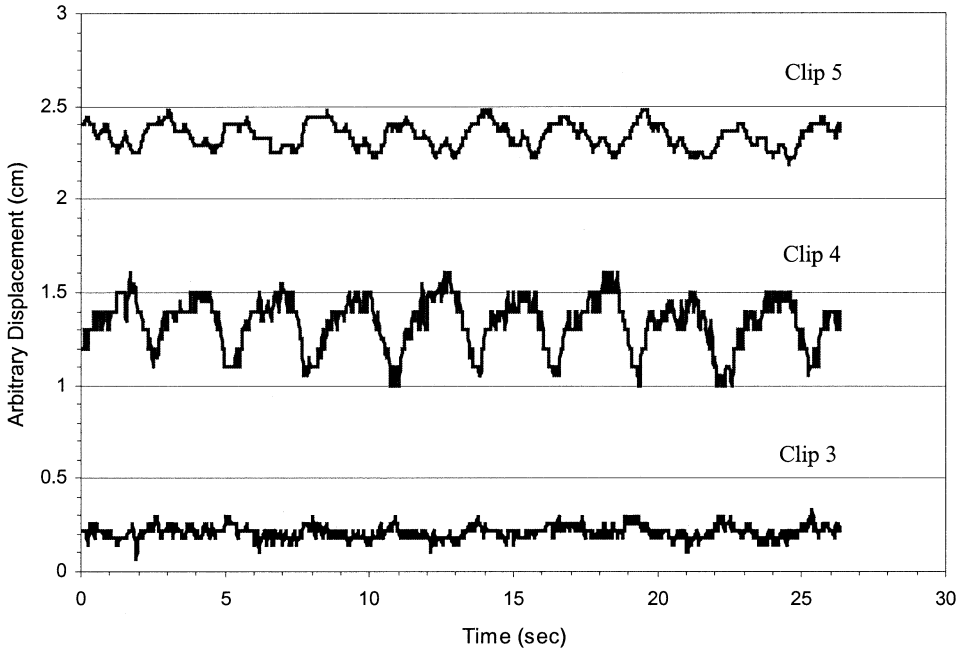

Fig. 9. Anterior-posterior clip motion as a function of time for Patient 5. Absolute values of clip displacements modified for display purposes.

had seven visible clips, each moving with different amplitudes. Although this does imply some degree of target deformation, the effective fluence algorithm models rigid body motion only, so the deformation was ignored in the treatment planning analysis. The target as a whole was assumed to move rigidly according to the motion data from Clip 1. This clip had the largest peak-to-peak amplitude and was chosen to observe the largest potential effect on the treatment plan. The average peak-to-peak motion in the CC and AP directions for Patient 1 was 9.6 mm and 6.9 mm, respectively.

For the pancreatic body tumor, motion comparisons using only CC motion, as well as both CC and AP motion, were performed to examine any dosimetric effect for each direction of motion. The IMRT plan for these 2 cases consisted of seven fields, each using 6-MV photons. The prescribed dose was 50.4 Gy, with a dose per fraction of 1.8 Gy. A PTV expansion of 8 mm around the CTV was used. Figure 10 shows the CTV DVH for 3 cases: without motion, with CC motion only, and with both CC and AP motion. The dosimetric impact for either motion case was small, and the two motion cases are very similar, differing only at high doses. The difference in volume coverage, at the prescription dose, was only 2–3% when including the effect of tumor motion. The target dose for this case was actually slightly greater when motion was included, which may occur because the target is moving into regions that contain hot spots.

A third comparison for Patient 1 was done using the actual tumor volume at the head of the pancreas. A 6-MV, seven-field IMRT plan was generated to a prescription dose of 45 Gy. Again, an 8-mm expansion to the PTV was used. Target motion was modeled in both the AP and the CC directions. The motion for Clip 1 was projected into the beam's eye view for each gantry angle to determine the lateral target motion for each treatment field. Figure 11 shows comparative DVHs for the CTV for IMRT plans with and without target motion. For this case, the target motion significantly perturbed the original DVH, leading a significant underdosing at the CTV. The inclusion of patient-specific motion in the treatment plan led to a 28% reduction in the amount of CTV receiving the prescription dose. Furthermore, the minimal CTV dose decreased by 8%.

A motion study was also done for Patient 2. This patient had average peak-to-peak motion in the CC and lateral directions of 8.1 mm and 3.9 mm, respectively, similar to the average amount of motion seen for the 7 patients included in this study. A six-field IMRT plan was generated using 6-MV photons. Two plans were generated, one without tumor motion and one using the effective fluence algorithm to estimate the effect of target motion. The target was assumed to move with the trajectory data from Clip 1. The effects of motion in both CC and AP directions were included. The resulting DVHs are shown in Fig. 12. The target motion for this patient had a modest effect on the CTV DVH. The minimal dose decreased by 2%, and the amount of volume receiving the prescription dose decreased by 7.5%.

The effects of target motion were also investigated for Patient 5. A seven-field, 6-MV plan was generated, and the motion data from Clip 3 was used, because this was the only clip that appeared in both the AP and the lateral fluoroscopic movies. This patient had a minimal amount of motion, with an average peak-to-peak motion of 4.7 mm and 2.5 mm in

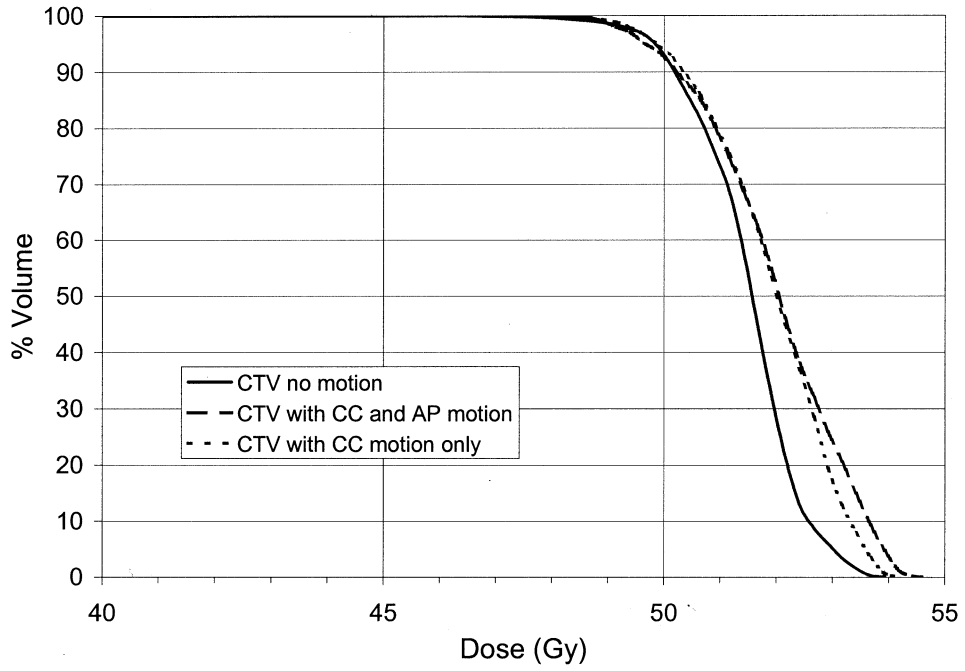

Fig. 10. Comparison of clinical target volume (CTV) dose volume histograms with and without target motion for Patient 1, artificial tumor of pancreas body only. Motion analysis included motion only in cranio-caudal (CC) direction. AP = anterior-posterior.

the CC and AP directions, respectively. Both directions of motion were included in the effective fluence calculation. The DVH comparison is shown in Fig. 13. The perturbation of the CTV for this case was negligible, with no change in the minimal CTV dose, and a 2% change in the volume of CTV receiving the prescription dose.

DISCUSSION

The results of this study indicate that fluoroscopic analysis of tumor motion is a useful tool in evaluating abdominal tumor motion. The magnitude of motion observed in this study was not inconsistent with other data

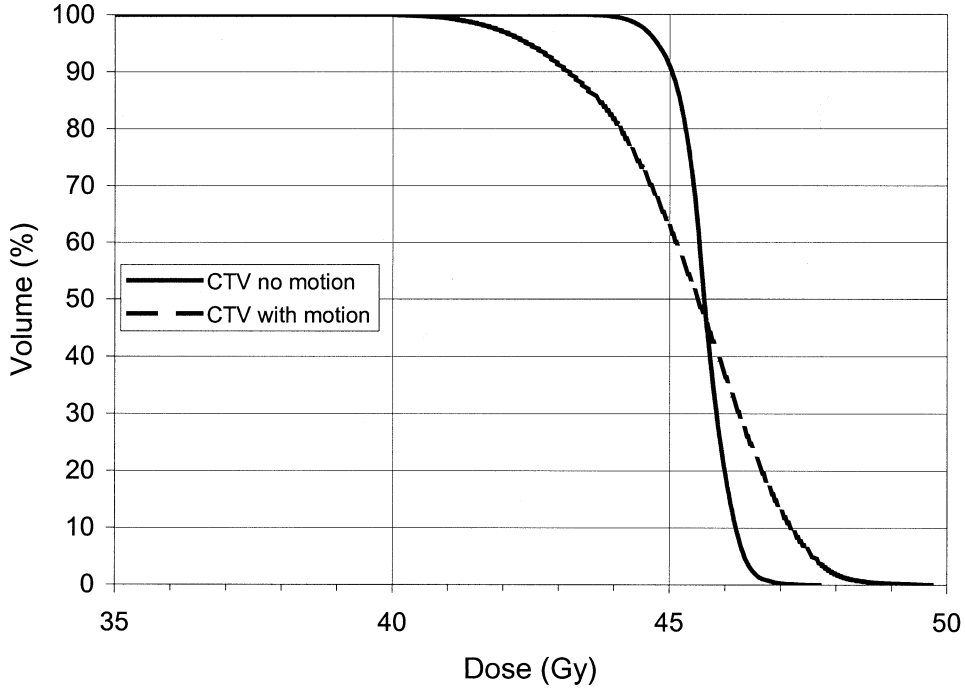

Fig. 11. Comparison of clinical target volume (CTV) dose volume histograms with and without target motion for Patient 1, large tumor located at head of pancreas.

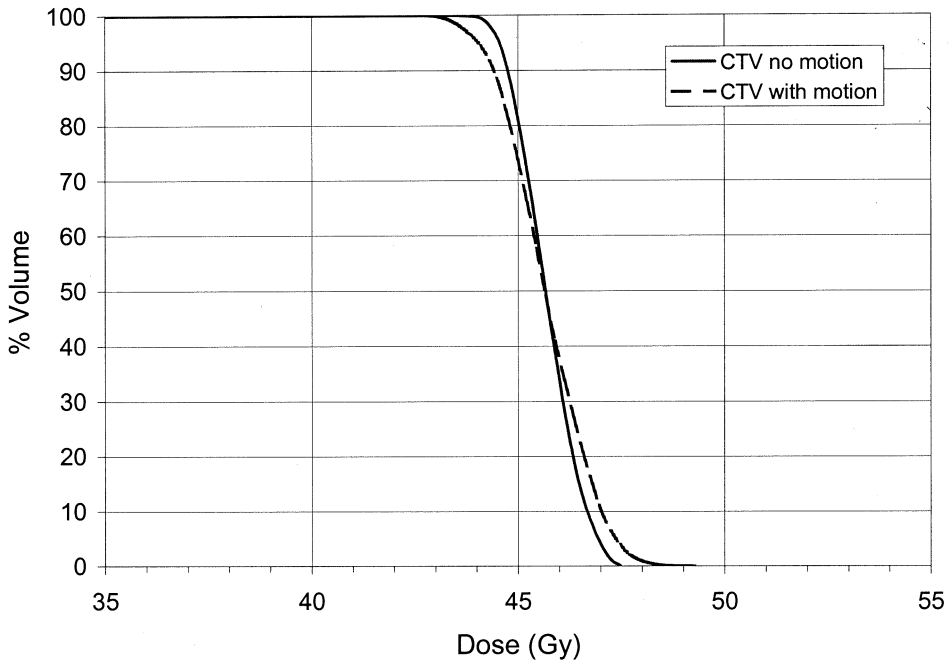

Fig. 12. Comparison of clinical target volume (CTV) dose volume histograms with and without target motion for Patient 2.

in the literature (19). Suramo *et al.* (20) used ultrasonography and found that the pancreas moved, on average, 2 cm (range 1–3) peak to peak craniocaudally. These data are for the body of the pancreas only, because the tail of the pancreas is difficult to locate with ultrasonography. Furthermore, that study did not include patients with pancreatic tumors. Kivisaari *et al.* (21) demonstrated that the pancreas is less mobile when a tumor is present, but the comparison was limited because only 2 patients with cancer of the pancreatic head were included in the anal-

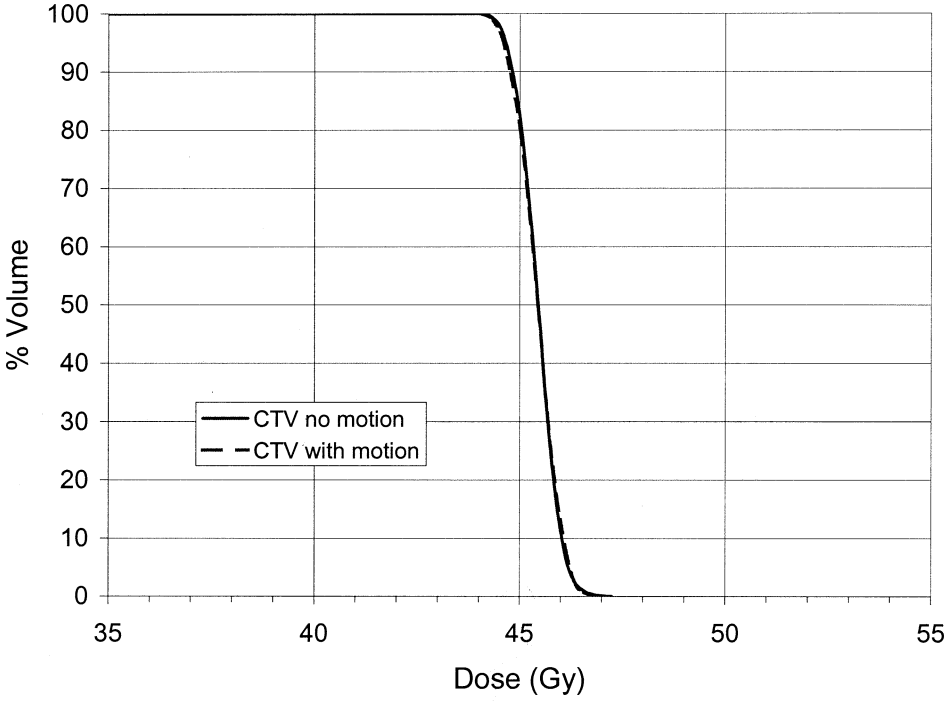

Fig. 13. Comparison of clinical target volume (CTV) dose volume histograms with and without target motion for Patient 5.

ysis. Bryan *et al.* (22) also examined pancreatic motion using ultrasonography and found that the body of the pancreas moved an average of 1.8 cm. Murphy *et al.* (23) used fluoroscopy to study the motion of implanted fiducial markers for 1 patient with a pancreatic tumor for the purposes of image-guided radiosurgery and observed motion in the inferior–superior direction to be about 5–10 mm. Patients were then treated under breath-hold conditions to minimize target motion; no analysis of the impact of target motion on the treatment was, therefore, necessary. More extensive information exists in the literature for the liver (19, 24). Several authors have investigated liver motion, with CC motion under normal breathing conditions in the range of 8–25-mm peak to peak. These studies used ultrasonography, MRI, technetium-99m uptake, and CT techniques to analyze liver and liver tumor motion; clip visualization, however, was not used.

Recently, four-dimensional CT has been demonstrated as a method for gathering organ motion data as a function of time (25–28). Fluoroscopic imaging of organ motion, such as the study presented here, provides complementary information to four-dimensional CT studies. Both are useful in evaluating organ motion and have applications in image-guided therapy. Four-dimensional CT may be susceptible to imaging artifacts under conditions of irregular breathing (25) (such as those observed in this study), and four-dimensional CT "movies," by virtue of the phase-correlated re-sorting, will be reduced to one "averaged" breathing cycle. The use of fluoroscopic imaging, used with computer vision techniques, enables organ motion data to be gathered continuously over many breathing cycles.

The limited number of patients in this study had average peak-to-peak motion of 7.4 $\pm$ 2.8 mm and 3.8 $\pm$ 1.5 mm in the CC and AP directions, respectively. The maximal amount of motion for each patient was nearly 50% greater than the average, indicating that significant deviations are possible, in terms of amplitude, during the average breathing cycle. The period of motion, however, was very stable, with a standard deviation of only 5%. Six of 7 patients had an average CC peak-to-peak motion of $<$1 cm, and five had a maximal CC peak-to-peak motion of $<$1 cm. Although it is obvious that some variation will occur in tumor motion from patient to patient, differences also will occur in clip motion for the same patient (i.e., different clips within the same patient can move different amounts). This raises the question of how to choose a representative marker to quantify or track the actual motion of the tumor. The motion seen for these abdominal patients, however, was relatively small compared with other sites, such as the lung, where the motion can be as much as 2–3 cm. As discussed below, however, abdominal tumor motion can still adversely impact target DVHs in some cases.

Results were given for IMRT motion comparisons for 3 patients (5 cases). For 2 patients (Patients 2 and 5), the effect of target motion was minimal and most likely clinically insignificant. Patient 5 had average clip motion of 4.7 mm and 2.5 mm in the CC and AP directions, respectively. As expected, the DVH for the CTV was not affected by including the tumor motion. Patient 2 had much larger motion in the CC direction, with an average clip motion of 8.1 mm. The effect of motion on the CTV DVH was still quite small (Fig. 12). Three comparisons were done for Patient 1. The first two used an artificial target of the pancreas only and included either CC motion only or both CC and AP motion; the second also included the tumor at the head of the pancreas (including both CC and AP motion). The CC motion for this patient was 9.6 mm on average, with a maximal motion of up to 18 mm, and the average AP motion was 6.9 mm. For the smaller tumor of the pancreas only, including the CC motion in the treatment plan led to only a minimal effect. The CTV DVH did not change significantly if AP motion was included in addition to the CC motion. This would suggest that, at least for this patient, most of the change in the target dose was caused by CC motion; the addition of AP motion was nearly insignificant. The third treatment planning comparison for Patient 1 (large tumor at head of pancreas; Fig. 11) showed a substantial change in the CTV DVH as a result of including the target motion. The tumor at the head of the pancreas was about 10 times larger than the volume of the artificial tumor (pancreas only). The magnitude of change in the CTV DVH may be influenced by the size of the tumor and also the specifics of each patient's treatment plan (e.g., degree of intensity modulation, resolution of intensity map, and interplay between target and leaf motion). For example, Patients 1 and 2 had, on average, similar magnitudes of target motion in the CC direction but the CTV DVH for Patient 2 was only changed minimally with the inclusion of target motion.

The potentially large change in the CTV DVH shown for Patient 1 indicate that some IMRT plans generated for patients with relatively large amounts of CC motion ($>$1 cm) may be susceptible to errors induced by tumor motion. The methods of analysis used in this study to determine potential changes in planned target DVHs may aid in the decision to use some form of motion mitigation or treatment intervention. For patients treated with respiratory gating using an external marker, a correlation between surface marker movement and internal anatomy is needed for reliable treatment and is the subject of ongoing study by us. Increasing the PTV margins would not have improved the target coverage for the DVHs shown in Fig. 11 for Patient 1. For motion with an average amplitude of 4.8 mm (9.6 peak to peak), a PTV expansion of 8 mm should be sufficient to cover the trajectory of the target adequately for static fields. For target motion that is encompassed by the PTV, an additional increase in the PTV margins will not improve target coverage. The effect is instead due to the interplay between multileaf collimator leaf motion and target motion.

It should be noted that these organ motion comparisons ignored the effect of variations in the phase at which treatment was initiated (i.e., the assumption was made that the beam was turned on at the same point in the breathing cycle for each fraction). This is similar to a gating scenario, in which the beam is synchronized with a particular phase of the breathing cycle. Bortfeld *et al.* (29) performed a statistical analysis and simulation study on the effects of intrafraction organ motion and demonstrated that the dose at a single point can vary with the initial phase of the breathing cycle. Furthermore, the vari-

ation in expected doses decreases significantly for fractionated RT compared with a dose delivered in a single fraction. The magnitude of the dose difference caused by organ motion, as well any effect of the initial phase, is also dependent on the treatment dose rate. These studies were done assuming an effective dose rate of 400 MU/min. Treating at a lower dose rate can smooth out errors (i.e., the target would be outside of its expected position for only a small portion of the treatment), because the beam is on longer. Longer treatment times also minimize the effect of the initial phase. For higher dose rates, the effects can be larger, because there is less time averaging during the treatment.

CONCLUSION

We studied the extent of tumor motion in the abdomen and explored the impact of tumor motion on IMRT dose distributions. Quantitative fluoroscopic analysis of patients with radiopaque tumor markers is useful in determining the characteristics of tumor motion. The amount of tumor motion for most patients in this study was not large, but could have, in some instances, significantly degraded the planned target DVH. The methods used in this study, therefore, are useful in determining whether motion mitigation or intervention strategies may be necessary.

REFERENCES

1. Balter JM, Lam KL, McGinn CJ, *et al.* Improvement of CT-based treatment planning models of abdominal targets using static exhale imaging. *Int J Radiat Oncol Biol Phys* 1998;41:939–943.
2. Wong JW, Sharpe MB, Jaffray DA, *et al.* The use of active breathing control (ABC) to reduce margin for breathing motion. *Int J Radiat Oncol Biol Phys* 1999;44:911–919.
3. Rosenzweig KE, Hanley J, Mah D, *et al.* The deep inspiration breath-hold technique in the treatment of inoperable non-small-cell lung cancer. *Int J Radiat Oncol Biol Phys* 2000;48: 81–87.
4. Barnes EA, Murray BR, Robinson DM, *et al.* Dosimetric evaluation of lung tumor immobilization using breath hold at deep inspiration. *Int J Radiat Oncol Biol Phys* 2001;50:1091–1098.
5. Kubo HD, Len RM, Minohara S, *et al.* Breathing-synchronized radiotherapy program at the University of California Davis Cancer Center. *Med Phys* 2000;27:346–353.
6. Ohara K, Okumura T, Akisada T, *et al.* Irradiation synchronized with respiration gate. *Int J Radiat Oncol Biol Phys* 1989;17:853–857.
7. Ford EC, Mageras GS, Yorke E, *et al.* Evaluation of respiratory movement during gated radiotherapy using film and electronic portal imaging. *Int J Radiat Oncol Biol Phys* 2002;52: 522–531.
8. Vedam SS, Keall PJ, Kini VR, *et al.* Determining parameters for respiration-gated radiotherapy. *Med Phys* 2001;28:2139–2146.
9. Jiang SB, Zygmanski P, Kung J, *et al.* Gated motion adaptive therapy (GMAT): Modification of IMRT MLC leaf sequence to compensate for tumor motion. *Med Phys* 2002;29:1347.
10. Shirato H, Shimizu S, Kunieda T, *et al.* Physical aspects of a real-time tumor-tracking system for gated radiotherapy. *Int J Radiat Oncol Biol Phys* 2000;48:1187–1195.
11. Keall PJ, Kini V, Vedam SS, *et al.* Motion adaptive X-ray therapy: A feasibility study. *Phys Med Biol* 2001;46:1–10.
12. Korevaar EW, Huizenga H, Lof J, *et al.* Investigation of the added value of high-energy electrons in intensity-modulated radiotherapy: Four clinical cases. *Int J Radiat Oncol Biol Phys* 2002;52:236–253.
13. Cheng JC-H, Wu J-K, Huang C-M, *et al.* Dosimetric analysis and comparison of three-dimensional conformal radiotherapy and intensity-modulated radiation therapy for patients with hepatocellular carcinoma and radiation-induced liver disease. *Int J Radiat Oncol Biol Phys* 2003;56:229–234.
14. Horn BKP. Robot vision. Cambridge, MA: MIT Press/ McGraw-Hill; 1986.
15. Haykin S. Adaptive filter theory. Upper Saddle River, NJ: Prentice Hall; 1991.
16. Kung JH, Zygmanski P, Choi N, *et al.* A method of calculating a lung clinical target volume DVH for IMRT with intrafractional motion. *Med Phys* 2003;30:1103–1109.
17. Zygmanski P, Kung J, Jiang S, *et al.* A novel method for calculating 3D dose error in IMRT treatment of lung cancer with and without respiratory gating. *Med Phys* 2001;28:1203.
18. Betke M, Makris NC. Recognition and complexity of objects subject to affine transformation. *Int J Comput Vis* 2001;44:5–40.
19. Langen KM, Jones DTL. Organ motion and its management. *Int J Radiat Oncol Biol Phys* 2001;50:265–278.
20. Suramo I, Paivansalo M, Myllyla V. Cranio-caudal movements of the liver, pancreas and kidneys in respiration. *Acta Radiol Diagn* 1984;25:129–131.
21. Kivisaari L, Makela P, Aarimaa M. Pancreatic mobility: An important factor in pancreatic computed tomography. *J Comput Assist Tomogr* 1982;6:854–856.
22. Bryan PJ, Custar S, Haaga JR, *et al.* Respiratory movement of the pancreas: An ultrasonic study. *J Ultrasound Med* 1984;3: 317–320.
23. Murphy MJ, Adler JR, Bodduluri M, *et al.* Image-guided radiosurgery for the spine and pancreas. *Comput Aid Surg* 2000;5:278–288.
24. Brock KK, Hollister SJ, Dawson LA, *et al.* Creating a 4D model of the liver using finite element analysis. *Med Phys* 2002;29:1403–1405.
25. Ford EC, Mageras GS, Yorke E, *et al.* Respiration-correlated spiral CT: A method of measuring respiratory-induced anatomic motion for radiation treatment planning. *Med Phys* 2003;30:88–97.
26. Vedam SS, Keall PJ, Kini VR, *et al.* Acquiring a four-dimensional computed tomography dataset using an external respiratory signal. *Phys Med Biol* 2003;48:45–62.
27. Low DA, Nystrom M, Kalinin E, *et al.* A method for the reconstruction of four-dimensional synchronized CT scans acquired during free breathing. *Med Phys* 2003;30:1254–1263.
28. Rietzel E, Doppke K, Pan T, *et al.* 4D computer tomography for treatment planning. *Int J Radiat Oncol Biol Phys.* 2003; 57:S232–S233.
29. Bortfeld T, Jokivarsi K, Goitein M, *et al.* Effects of intrafraction motion on IMRT dose delivery: Statistical analysis and simulation. *Phys Med Biol* 2002;47:2203–2220.